Supporting Information for

"Direct Simulation of Excited-State Intramolecular Proton Transfer and Vibrational Coherence of 10-Hydroxybenzo[h]quinoline in Solution"

Masahiro Higashi and Shinji Saito

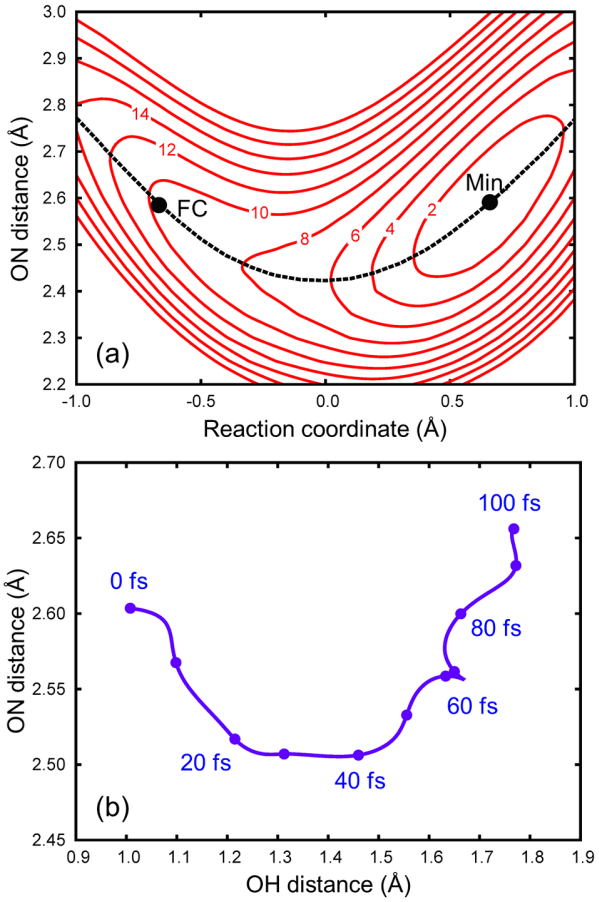

Figure S1. (a) Two-dimensional potential energy surface in terms of the reaction coordinate and ON distance. Contours are spaced from 2 to 20 kcal/mol in intervals of 2 kcal/mol, where the zero of the energy is set at the minimum S_1 energy. The black dashed line shows the minimum-energy path, and FC and Min represent the Frank-Condon and minimum energy points, respectively. (b) The averaged trajectory up to 100 fs on the two-dimensional plot in terms of the OH and ON distances. Dots indicate the position of the averaged trajectory placed every 10 fs.

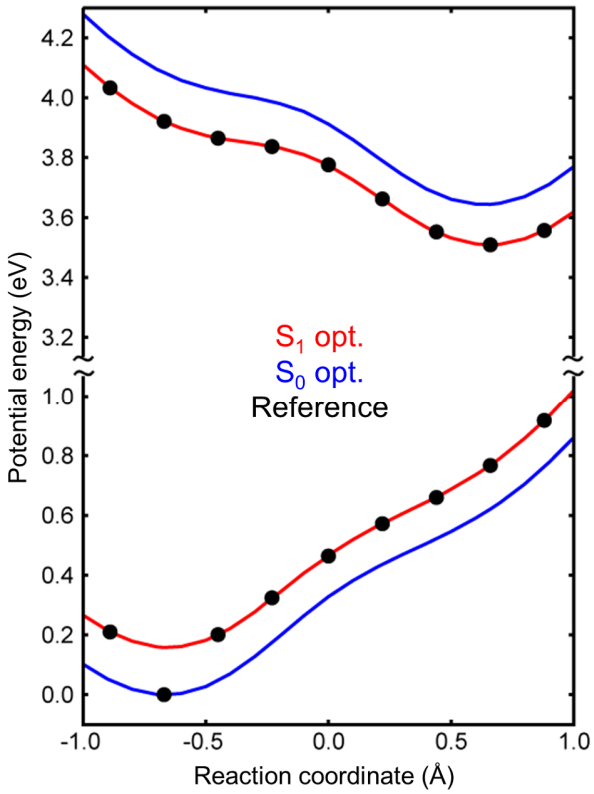

Figure S2. The potential energy profiles of the ground and excited states along the reaction coordinate (red and blue lines, which are those that are optimized on the excited and ground potential energy surfaces) and the locations of the reference geometries (black dots).

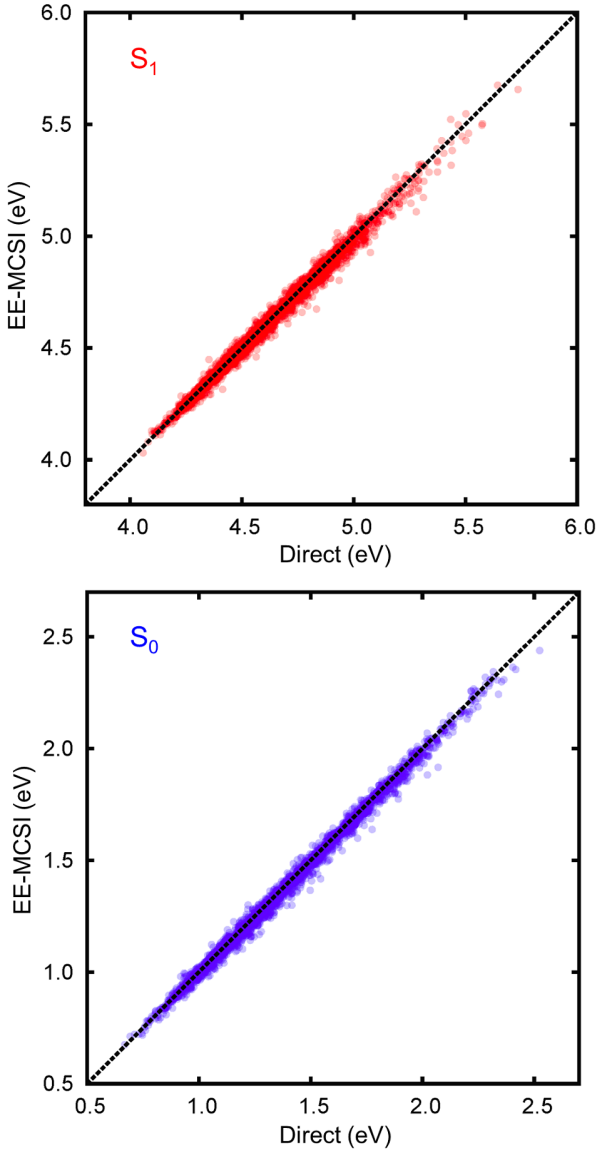

Figure S3. Comparison between the EE-MCSI and direct energies at 2200 configurations: the excited-state (top) and ground-state (bottom) energy.

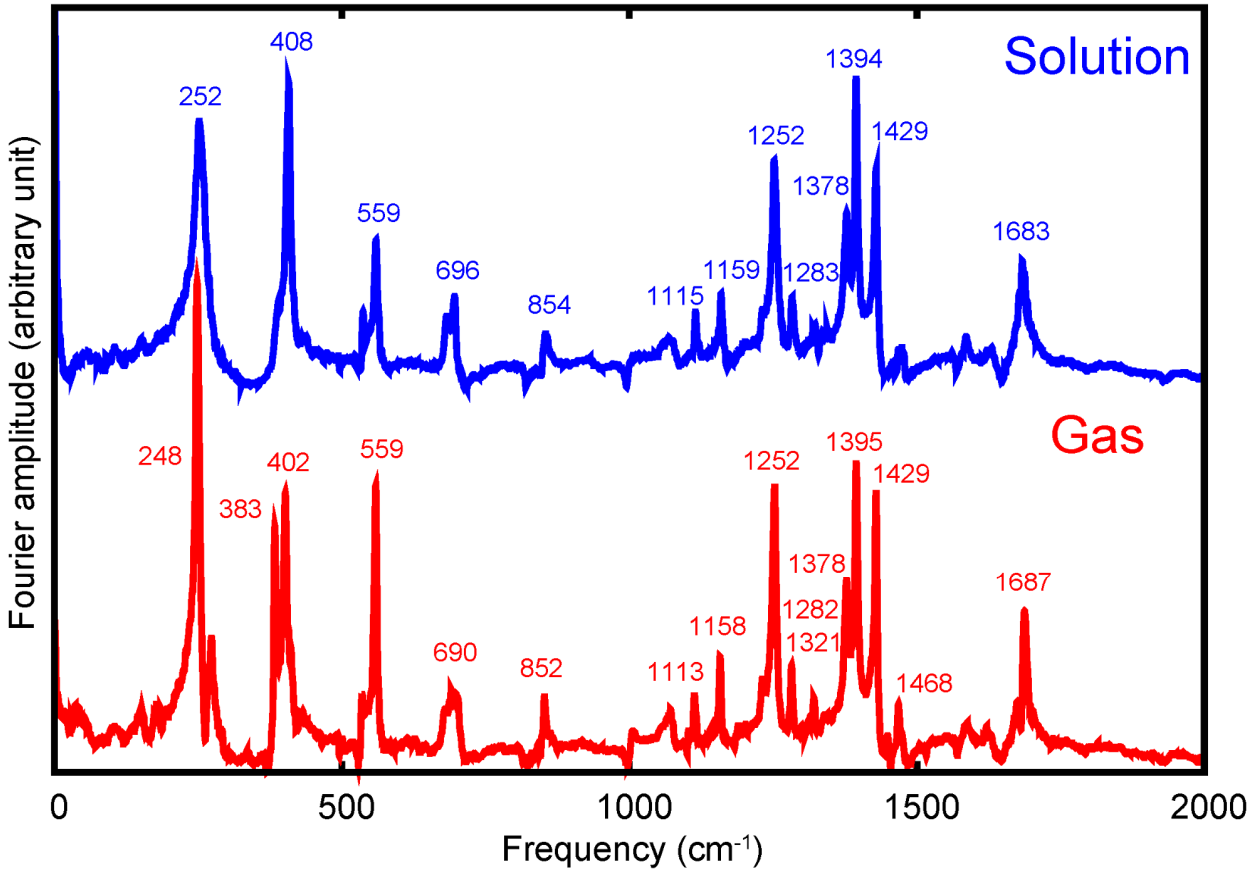

Figure S4. Calculated Fourier amplitude spectra of the oscillatory components of the energy gap up to 2000 cm^{-1} in solution (an offset is added) and in the gas phase.

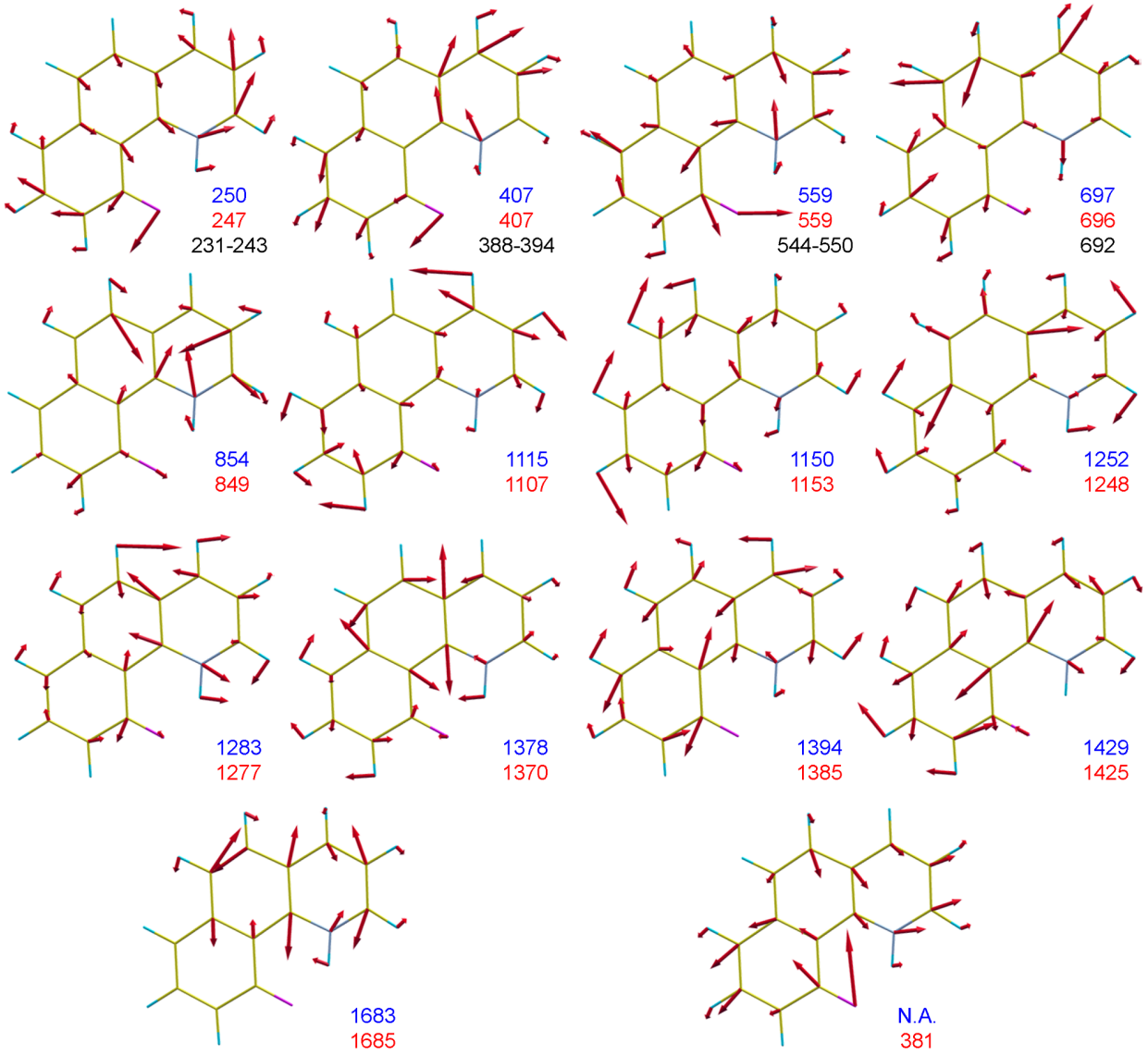

Figure S5. Normal modes calculated at the excited-state minimum geometry for coherent vibrational modes. Blue, red, and black numbers are frequencies calculated from the simulation, normal-mode frequencies, and experimental frequencies, respectively (in cm^{-1}). The mode at ~380 cm^{-1} is found only in the gas-phase reaction. Displacement vectors are presented in mass-weighted.

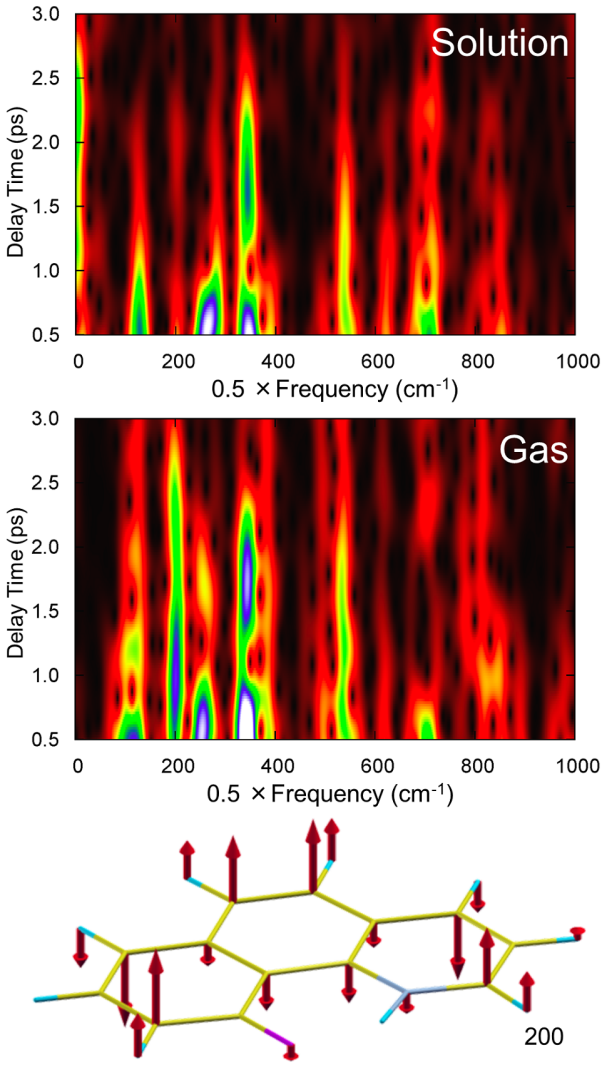

Figure S6. Sliding-Fourier transform analysis of the oscillatory components of the S_1 potential energy of 10-HBQ: in solution (top) and the gas phase (middle). Notably, the frequency was divided in half due to the symmetry of the potential energy. Normal mode at the excited-state optimized geometry for the out-of-plane mode at 200 cm^{-1} (bottom).

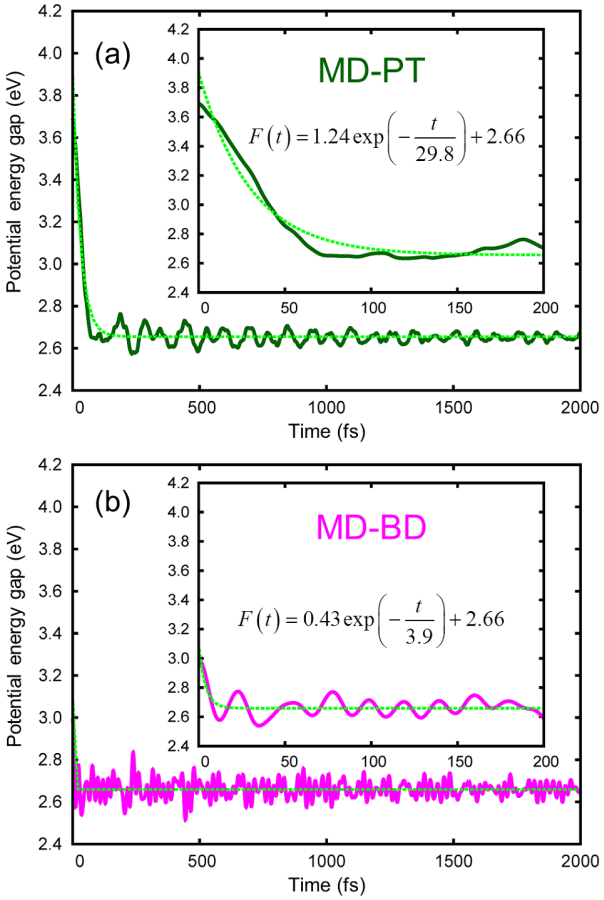

Figure S7. Time evolution of the averaged potential energy gap between the ground and excited states calculated from the simulations of (a) MD-PT and (b) MD-BD.

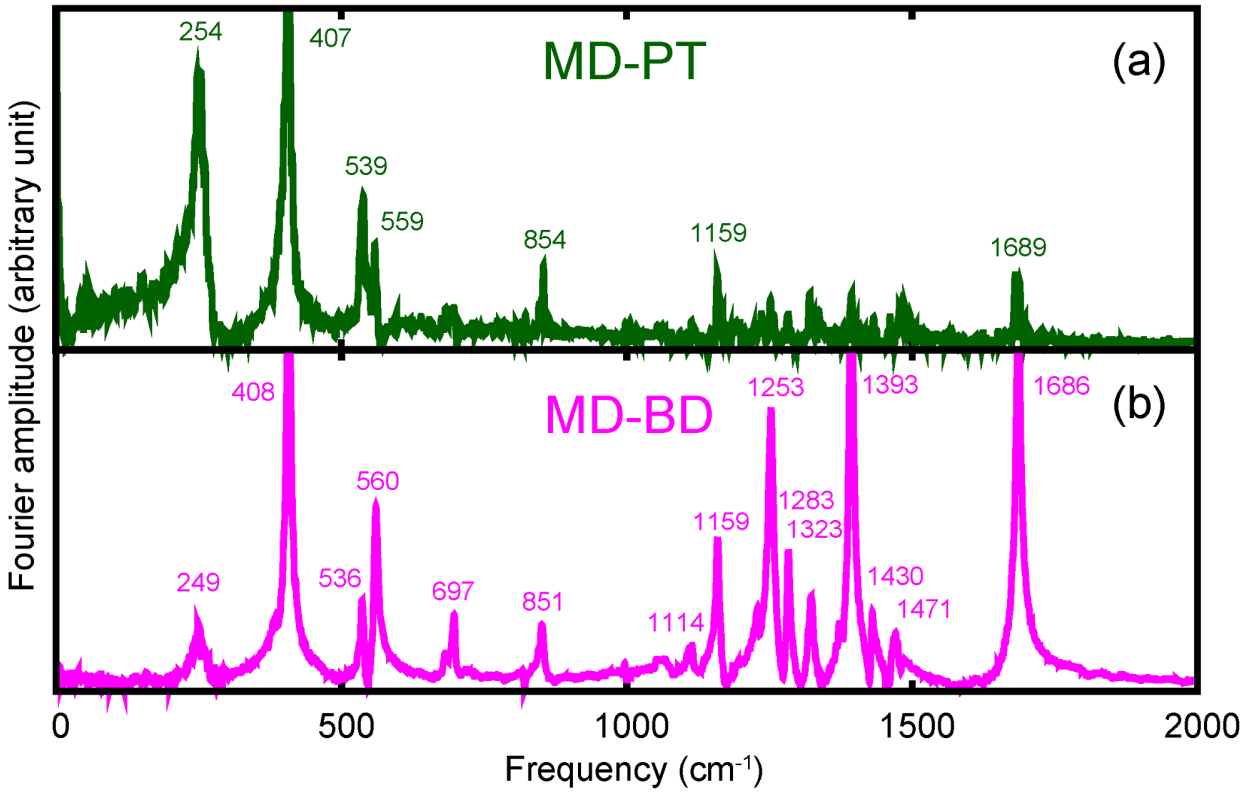

Figure S8. Fourier amplitude spectra of the oscillatory components of the energy gap calculated from the simulations of (a) MD-PT and (b) MD-BD up to 2000 cm^{-1}.

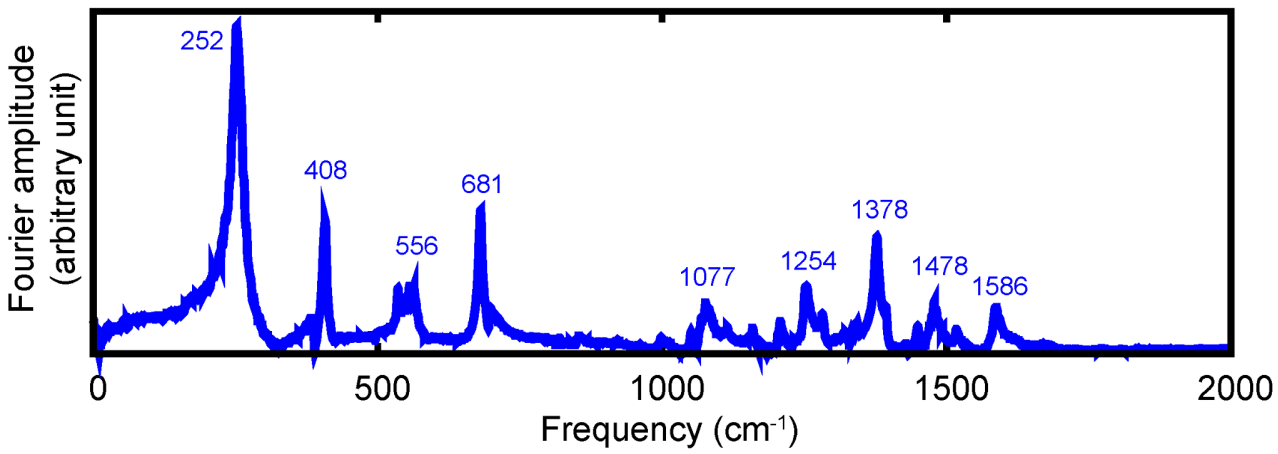

Figure S9. Fourier amplitude spectrum of the oscillatory component of the averaged reaction coordinates.

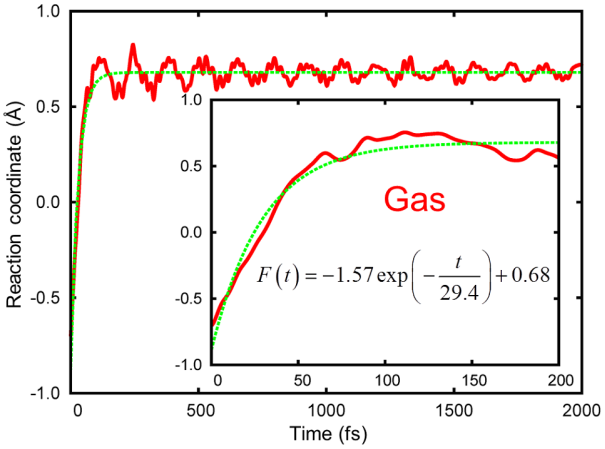

Figure S10. Time evolution of the averaged reaction coordinate in the gas phase.

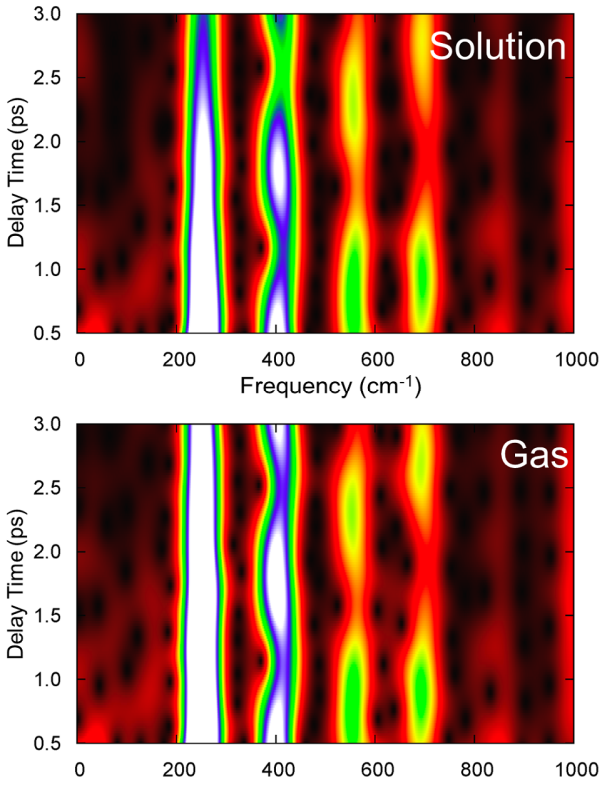

Figure S11. Sliding-Fourier transform analysis of the oscillatory component of the energy gap from the simulations with all the torsional angles restrained: in solution (top) and in the gas phase (bottom)

Table S1. Errors (kcal/mol) during MD simulations[a]

z_C	excited state			ground state		
	MSE	MUE	RMSE	MSE	MUE	RMSE
−1.0	0.0	0.4	0.5	−0.1	0.4	0.5
−0.9	−0.3	0.6	0.7	−0.4	0.6	0.8
−0.8	−0.1	0.5	0.6	−0.2	0.4	0.6
−0.7	−0.2	0.6	0.8	−0.2	0.7	0.9
−0.6	−0.3	0.5	0.7	−0.3	0.6	0.8
−0.5	−0.1	0.5	0.5	−0.2	0.4	0.5
−0.4	−0.2	0.6	0.7	−0.4	0.5	0.7
−0.3	−0.2	0.5	0.7	−0.4	0.5	0.7
−0.2	−0.3	0.7	1.0	−0.4	0.7	0.9
−0.1	−0.2	0.4	0.5	−0.3	0.4	0.5
0.0	−0.1	0.4	0.6	−0.2	0.4	0.5
0.1	−0.2	0.5	0.7	−0.3	0.5	0.6
0.2	−0.1	0.4	0.5	−0.2	0.4	0.5
0.3	−0.2	0.5	0.8	−0.3	0.5	0.7
0.4	−0.2	0.4	0.5	−0.3	0.4	0.5
0.5	−0.2	0.5	0.6	−0.3	0.5	0.6
0.6	−0.2	0.5	0.6	−0.2	0.4	0.5
0.7	−0.1	0.4	0.6	−0.2	0.4	0.6
0.8	−0.2	0.4	0.5	−0.1	0.4	0.5
0.9	−0.1	0.4	0.4	−0.2	0.3	0.4
1.0	−0.1	0.5	0.7	−0.2	0.5	0.7
S_0[b]	−0.4	0.7	0.9	−0.3	0.6	0.8
all	−0.2	0.5	0.7	−0.3	0.5	0.6

[a] MSE, MUE, and RMSE denote the mean signed error, mean unsigned error, and root-mean-square error, respectively.

[b] ground-state MD simulation without restraint.

Table S2. Decay times of the vibrational modes calculated from the simulations with all of the torsional angles restrained (in ps)

frequency (cm^{-1})	solution	gas
~250	2.90	4.68
~400	4.94	11.27
~550	10.16	6.03

Table S3. All of the internal coordinates used in the Taylor expansions of the EE-MCSI calculations[a].

type	internal coordinates
bond	1-22 21-22 1-21 1-2 1-24 2-3 2-4 4-5 4-6 6-7 6-8 8-9 8-24 9-10 9-11 11-12 11-13 13-14 13-23 14-15 14-16 16-17 16-18 18-19 18-20 20-21 20-23 23-24
angle	2-1-22 2-1-24 22-1-24 1-2-3 1-2-4 3-2-4 2-4-5 2-4-6 5-4-6 4-6-7 4-6-8 7-6-8 6-8-9 6-8-24 9-8-24 8-9-10 8-9-11 10-9-11 9-11-12 9-11-13 12-11-13 11-13-14 11-13-23 14-13-23 13-14-15 13-14-16 15-14-16 14-16-17 14-16-18 17-16-18 16-18-19 16-18-20 19-18-20 18-20-21 18-20-23 21-20-23 20-21-22 13-23-20 13-23-24 20-23-24 1-24-8 1-24-23 8-24-23
improper	24-2-1-22 22-24-1-2 2-22-1-24 4-3-2-1 3-1-2-4 1-4-2-3 2-6-4-5 6-5-4-2 5-2-4-6 8-4-6-7
torsion	4-7-6-8 7-8-6-4 9-24-8-6 24-6-8-9 6-9-8-24 8-11-9-10 11-10-9-8 10-8-9-11 9-13-11-12 13-12-11-9 12-9-11-13 11-14-13-23 14-23-13-11 23-14-13-11 13-16-14-15 16-15-14-13 15-13-14-16 14-18-16-17 18-17-16-14 17-14-16-18 20-16-18-19 16-19-18-20 19-20-18-16 23-18-20-21 18-21-20-23 21-23-20-18 20-13-23-24 13-24-23-20 24-20-23-13 8-23-24-1 23-1-24-8 1-8-24-23
torsion	22-1-2-3 22-1-2-4 24-1-2-3 24-1-2-4 2-1-24-8 2-1-24-23 2-22-1-24-8 22-1-24-23 1-2-4-5 1-2-4-6 3-2-4-5 3-2-4-6 2-4-6-7 2-4-6-8 5-4-6-7 5-4-6-8 4-6-8-9 4-6-8-24 7-6-8-9 7-6-8-24 6-8-9-10 6-8-9-11 24-8-9-10 24-8-9-11 6-8-24-1 6-8-24-23 9-8-24-1 9-8-24-23 8-9-11-12 8-9-11-13 10-9-11-12 10-9-11-13 9-11-13-14 9-11-13-23 12-11-13-14 12-11-13-23 11-13-14-15 11-13-14-16 23-13-14-15 23-13-14-16 11-13-23-20 11-13-23-24 14-13-23-20 14-13-23-24 13-14-16-17 13-14-16-18 15-14-16-17 15-14-16-18 14-16-18-19 14-16-18-20 17-16-18-19 17-16-18-20 16-18-20-21 16-18-20-23 19-18-20-21 19-18-20-23 18-20-21-22 23-20-21-22 18-20-23-13 18-20-23-24 21-20-23-13 21-20-23-24 13-23-24-1 13-23-24-8 20-23-24-1 20-23-24-8

[a] The atom numbering is as shown in figure below.

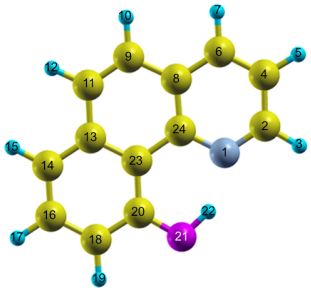

Computational Details

Electronic Structure Calculations

For the reference electronic structure calculation of the EE-MCSI method, we used the density functional theory and time-dependent density functional theory for the ground and excited states. Notably, the calculated results such as the shape of the spectrum and the decay times of the vibrational modes strongly depend on the density functional used. The details of the density functional dependence are described elsewhere.[1] Here we showed the best results among the calculations with various density functionals. We used the LC-BOP functional with the parameter μ=0.33.[2,3] The basis set was 6-31+G(d,p) for N and O atoms, and 6-31G(d,p) for C and H atoms. The absorption and fluorescence energies calculated at this level are 4.08 and 2.74 eV, which are larger than the experimental energies,[4] 3.26 and 1.98 eV, respectively. However, the calculated difference between the absorption and fluorescence energies (1.34 eV) is in good agreement with the experimentally determined difference (1.28 eV). We define the reaction coordinate as the difference between breaking O-H and forming N-H bonds:

$$z = R_{\mathrm{OH}} - R_{\mathrm{NH}}. \tag{S1}$$

The projector operator method[5] was used to optimize geometries along the reaction coordinate. We adopted the RESP charge model[6] to describe the electrostatic distribution of the 10-HBQ molecule, where the grid points were generated by using an algorithm proposed by Spackman[7] (GAMESS[8] default); and harmonic restraints with constants of 1.0×10^{-3} a.u. were imposed on all of the atoms. All of the electronic structure calculations were performed using GAMESSPLUS[9] software based on the GAMESS quantum package[8], where we implemented our routines.

EE-MCSI method

We used the non-Hermitian EE-MCSI method to generate the global potential energy function of the ESIPT reaction of 10-HBQ. The non-Hermitian EE-MCSI method is a straightforward expansion of the non-Hermitian MCSI[10] and Hermitian EE-MCSI.[11] We constructed the diagonal elements H_{11} and H_{22} based on the AMBER GAFF force field version 1.4[12,13], and added the following two modifications,

(1) The bond stretching terms. We used Morse potentials instead of harmonic potentials to describe the forming N-H_N and breaking O-H_O bonds. The dissociation energies of the Morse potential were set equal to 86.7 and 115.7 kcal/mol for the O-H_O and N-H_N bonds, respectively, which were obtained from the experimental dissociation energy for the O-H bond in phenol[14] and proton affinity of pyridine.[15]

(2) The van der Waals (vdW) potential terms. In the original GAFF, the Lennard-Jones 12-6 type function is used for the vdW interactions,

$$V^{\mathrm{LJ}}(R) = \varepsilon_0 \left[\left(\frac{R_0}{R} \right)^{12} - 2 \left(\frac{R_0}{R} \right)^{6} \right], \tag{S2}$$

where R, ε_0, and R_0 are the distance between interacting atoms, the vdW well depth, and the vdW radius, respectively. We replaced it with the exponential-6 form,[16]

$$V^{\mathrm{X6}}(R) = \varepsilon_0 \left[\left(\frac{6}{\zeta - 6} \right) e^{\zeta \left(1 - \frac{R}{R_0} \right)} - \left(\frac{\zeta}{\zeta - 6} \right) \left(\frac{R_0}{R} \right)^{6} \right], \tag{S3}$$

where the parameter ζ was set equal to 12.0[16] in this work. Furthermore, as in previous MCSI and EE-MCSI studies,[17,18] we added an R^{-12} repulsive term to V^{X6},

$$V^{\mathrm{vdW}}(R) = V^{\mathrm{X6}}(R) + DE \left(\frac{R_0}{R} \right)^{12}, \tag{S4}$$

where

$$E = \left. \frac{V^{\mathrm{X6}}(R)}{\left(\frac{R_0}{R}\right)^{12}} \right|_{R=0.5R_0} \tag{S5}$$

and the parameter D was set equal to 0.01.[18] We also modified the vdW parameter for the H_O and H_N atoms because we found that the default vdW radii (0.0 and 0.6 Å for H_O and H_N) were too small to describe the repulsion between the proton and backbone carbon atom of 10-HBQ around z = 0.0. We used $R_0(H_O) = R_0(H_N) = 1.2$ Å and $\varepsilon_0(H_O) = \varepsilon_0(H_N) = 0.157$ kcal/mol (the latter is the default for H_N) .

These modifications were required to describe the behavior of the H_{11} and H_{22} properly in the region far from their minima. Note that, when we adopted these modifications, the parameters' dependence on the EE-MCSI potential energy function is quite small because the off-diagonal element H_{12} is determined to reproduce the reference energy in the presence of the given H_{11} and H_{22}. In fact, we obtained similar results when we set $0.8 \leq R_0(H_O) = R_0(H_N) \leq 1.6$ Å.

We took 9 reference geometries with evenly spaced reaction coordinates $\{z_k; k = 1, 2, \ldots, 9\}$ (Figure S2),

$$z_k = z_0 + \frac{8-k}{6}(z_1 - z_0), \tag{S6}$$

where z_0 and z_1 are the reaction coordinates at the ground and excited optimized geometries; i.e., $z_0 = -0.670$ and $z_1 = 0.660$ Å, respectively. We mainly used the excited-state geometries in constructing both the ground-state and excited-state EE-MCSI potential energy functions, but we used the ground-state geometry for k = 8 (the ground-state minimum) to construct the ground-state EE-MCSI potential energy function because we carried out the ground-state MD simulation around the minimum to prepare the initial configurations. Notably, the number of reference geometries can be reduced without losing a considerable amount of accuracy. However, we did not optimize the number of reference geometries because the purpose of this study is to describe the potential energy surface calculated by the reference electronic structure calculation as best as possible and not to reduce the computational cost as much as possible.

The off-diagonal element H_{12} was determined by using the quadratic Taylor expansions in internal coordinates and external electrostatic potentials on atomic sites. We used 179 redundant internal coordinates: 28 bonds, 43 angles, 42 improper torsions, and 66 torsions (Table S3). For improper torsions and torsions $\{\phi_m\}$, we replaced $\phi_m - \phi_m^{(k)}$ in the Taylor expansions ($\phi_m^{(k)}$ is the torsional angle at the reference geometry k) with $\frac{\sin\left(n_m\left(\phi_m - \phi_m^{(k)}\right)\right)}{n_m}$, where the periodicity n_m was set equal to 1 and 2 for improper torsions and torsions, respectively (see Ref. 19 and the manual of MCSI version 2010[20]). We used the same weight function for the breaking O-H_O and forming N-H_N bonds as has been used in the previous studies.[17] All of the EE-MCSI calculations were carried out using the MCSI program package.[20,21]

EE-MCSI/MM MD simulation

To consider solvent effects, the EE-MCSI potential energy functions mentioned above were combined with molecular mechanics as in the conventional combined quantum mechanical and molecular mechanical (QM/MM) method.[22] We prepared a cubic unit cell with a box length of 34.2 Å and periodic boundary conditions; the unit cell contains one 10-HBQ molecule and 215 cyclohexane molecules. The OPLS-AA force field[23,24] was used for cyclohexane. The vdW interaction between 10-HBQ and cyclohexane was also treated by the OPLS-AA force field. For the long-range electrostatic interaction, we used the tapering method implemented in the TINKER program,[21] where the electrostatic interaction smoothly becomes zero at 12 Å. A cutoff length of 12 Å was also used for the vdW interactions. The equations of motion were integrated using the leap-frog algorithm with a time step of 0.5 fs at a temperature of 300 K. In the MD-PT and MD-BD simulations (see main text), we added harmonic restraints on the reaction coordinate with a force constant 300 kcal/(mol Å^2). In restraining all of the torsional angles (including the improper torsions) in Table S2, a force constant of 300 kcal/(mol rad^2) was employed. All of the EE-MCSI/MM MD simulations were carried out using the AMBERPLUS program package.[13,25]

Error estimation of the EE-MCSI potential energy functions

The error in the EE-MCSI potential energy functions was estimated by performing the restrained excited-state MD simulations. We carried out 21 sets of excited-state MD simulations for 20 ps with a harmonic restraint $V^{\mathrm{rst}}(z) = K(z - z_{\mathrm{C}})^2$, where K = 100 kcal/(mol Å^2) and z_{C} = −1.0, −0.9, …, 1.0. In addition, we carried out a ground-state MD simulation for 20 ps without restraint to estimate the error during the ground-state MD simulation in preparing the initial configurations. The errors between the EE-MCSI and reference energies of the ground and excited states were estimated with 2200 configurations which were saved every 0.1 ps in the last 10 ps of 21 excited and 1 ground-state MD simulations. These results are summarized in Table S1 and Figure S3. The errors were quite small along the entire reaction coordinate. The mean unsigned error calculated from all of the configurations was 0.5 kcal/mol for both the excited and ground states.

References

(1) Higashi, M.; Saito, S., to be published.

(2) Iikura, H.; Tsuneda, T.; Yanai, T.; Hirao, K. A Long-Range Correction Scheme for Generalized-Gradient-Approximation Exchange Functionals. *J. Chem. Phys.* **2001**, *115*, 3540-3544.

(3) Chiba, M.; Tsuneda, T.; Hirao, K. Excited State Geometry Optimizations by Analytical Energy Gradient of Long-Range Corrected Time-Dependent Density Functional Theory. *J. Chem. Phys.* **2006**, *124*, 144106.

(4) Schriever, C.; Barbatti, M.; Stock, K.; Aquino, A. J. A.; Tunega, D.; Lochbrunner, S.; Riedle, E.; de Vivie-Riedle, R.; Lischka, H. The Interplay of Skeletal Deformations and Ultrafast Excited-State Intramolecular Proton Transfer: Experimental and Theoretical Investigation of 10-Hydroxy-benzo[h]quinoline. *Chem. Phys.* **2008**, *347*, 446-461.

(5) Lu, D. H.; Zhao, M.; Truhlar, D. G. Projection Operator Method for Geometry Optimization with Constraints. *J. Comput. Chem.* **1991**, *12*, 376-384.

(6) Bayly, C. I.; Cieplak, P.; Cornell, W. D.; Kollman, P. A. A Well-Behaved Electrostatic Potential

Based Method Using Charge Restraints for Deriving Atomic Charges - the Resp Model. *J. Phys. Chem.* **1993**, *97*, 10269-10280.

(7) Spackman, M. A. Potential Derived Charges Using a Geodesic Point Selection Scheme. *J. Comput. Chem.* **1996**, *17*, 1-18.

(8) Schmidt, M. W.; Baldridge, K. K.; Boatz, J. A.; Elbert, S. T.; Gordon, M. S.; Jensen, J. H.; Koseki, S.; Matsunaga, N.; Nguyen, K. A.; Su, S. J. et al. General Atomic and Molecular Electronic-Structure System. *J. Comput. Chem.* **1993**, *14*, 1347-1363.

(9) Higashi, M.; Marenich, A. V.; Olson, R. M.; Chamberlin, A. C.; Pu, J.; Kelly, C. P.; Thompson, J. D.; Xidos, J. D.; Li, J.; Zhu, T. et al. *GAMESSSPLUS*, *version 2010-2*; University of Minnesota: Minneapolis, MN, 2010.

(10) Tishchenko, O.; Truhlar, D. G. Non-Hermitian Multiconfiguration Molecular Mechanics. *J. Chem. Theory Comput.* **2009**, *5*, 1454-1461.

(11) Higashi, M.; Truhlar, D. G. Electrostatically Embedded Multiconfiguration Molecular Mechanics Based on the Combined Density Functional and Molecular Mechanical Method. *J. Chem. Theory Comput.* **2008**, *4*, 790-803.

(12) Wang, J. M.; Wolf, R. M.; Caldwell, J. W.; Kollman, P. A.; Case, D. A. Development and Testing of a General Amber Force Field. *J. Comput. Chem.* **2004**, *25*, 1157-1174.

(13) Case, D. A.; Darden, T. A.; Cheatham, I., T. E.; Simmerling, C. L.; Wang, J.; Duke, R. E.; Luo, R.; Walker, R. C.; Zhang, W.; Merz, K. M. et al. *AMBER, version 11*; University of California: San Francisco, CA, 2010.

(14) Mulder, P.; Korth, H. G.; Pratt, D. A.; DiLabio, G. A.; Valgimigli, L.; Pedulli, G. F.; Ingold, K. U. Critical Re-evaluation of the O-H Bond Dissociation Enthalpy in Phenol. *J. Phys. Chem. A* **2005**, *109*, 2647-2655.

(15) Hodges, R. V.; Beauchamp, J. L.; Ashe, A. J.; Chan, W. T. Proton Affinities of Pyridine, Phosphabenzene, and Arsabenzene. *Organometallics* **1985**, *4*, 457-461.

(16) Rappe, A. K.; Casewit, C. J.; Colwell, K. S.; Goddard, W. A.; Skiff, W. M. Uff, a Full Periodic-Table Force-Field for Molecular Mechanics and Molecular-Dynamics Simulations. *J. Am. Chem. Soc.* **1992**, *114*, 10024-10035.

(17) Kim, Y.; Corchado, J.; Villa, J.; Xing, J.; Truhlar, D. G. Multiconfiguration Molecular Mechanics Algorithm for Potential Energy Surfaces of Chemical Reactions. *J. Chem. Phys.* **2000**, *112*, 2718-2735.

(18) Tishchenko, O.; Truhlar, D. G. Optimizing the Performance of the Multiconfiguration Molecular Mechanics Method. *J. Phys. Chem. A* **2006**, *110*, 13530-13536.

(19) Higashi, M.; Truhlar, D. G. Efficient Approach to Reactive Molecular Dynamics with Accurate Forces. *J. Chem. Theory Comput.* **2009**, *5*, 2925-2929.

(20) Tishchenko, O.; Higashi, M.; Albu, T. V.; Corchado, J. C.; Kim, Y.; Villà, J.; Xing, J.; Lin, H.; Truhlar, D. G.; *MCSI, version 2010*; University of Minnesota: Minneapolis, MN, 2010.

(21) Ponder, J. W.;*TINKER, version 3.5*; Washington University: St. Louis, MO, 1997.

(22) Higashi, M.; Truhlar, D. G. Combined Electrostatically Embedded Multiconfiguration Molecular Mechanics and Molecular Mechanical Method: Application to Molecular Dynamics Simulation of a Chemical Reaction in Aqueous Solution with Hybrid Density Functional Theory. *J. Chem. Theory Comput.* **2008**, *4*, 1032-1039.

(23) Jorgensen, W. L.; Maxwell, D. S.; Tirado-Rives, J. Development and Testing of the OPLS All-Atom Force Field on Conformational Energetics and Properties of Organic Liquids. *J. Am. Chem. Soc.* **1996**, *118*, 11225-11236.

(24) Price, M. L. P.; Ostrovsky, D.; Jorgensen, W. L. Gas-Phase and Liquid-State Properties of Esters, Nitriles, and Nitro Compounds with the OPLS-AA Force Field. *J. Comput. Chem.* **2001**, *22*, 1340-1352.

(25) Higashi, M.; Truhlar, D. G.; *AMBERPLUS, version 2010*; University of Minnesota: Minneapolis, MN, 2010.